Ocean biogeochemical signatures of the North Pacific Blob

Samuel C. Mogen[1], Nicole S. Lovenduski[1], Allysa R. Dallmann[2], Luke Gregor[3], Adrienne J. Sutton[4], Steven J. Bograd[5], Nathali Cordero Quiros[5,7], Emanuele Di Lorenzo[8], Elliott L. Hazen[5], Michael G. Jacox[5,6], Mercedes Pozo Buil[5,7], Stephen Yeager [9]

[1]Department of Atmospheric and Oceanic Sciences and Institute of Arctic and Alpine Research, University of Colorado, Boulder, CO, USA
[2]Jackson School of Geosciences, University of Texas at Austin, Austin, Texas, USA
[3]Institute of Biogeochemistry and Pollutant Dynamics, ETH Zurich, Zurich, Switzerland
[4]National Oceanic and Atmospheric Administration Pacific Marine Environmental Lab, Seattle, WA, USA
[5]National Oceanic and Atmospheric Administration Southwest Fisheries Science Center, Monterey, CA, USA
[6]National Oceanic and Atmospheric Administration Physical Sciences Laboratory, Boulder, CO, USA
[7]Institute of Marine Sciences, University of California, Santa Cruz, CA, USA
[8]School of Earth and Atmospheric Science, Georgia Tech, Atlanta, GA, USA
[9]National Center for Atmospheric Research Climate and Global Dynamics Lab, Boulder, CO, USA

Key Points:

- The North Pacific Blob had a distinct biogeochemical signature that is captured by observations and multiple ocean models
- The Blob was characterized by anomalously high aragonite saturation states and anomalously low oxygen concentrations
- The biogeochemical Blob signature was driven by changes in temperature and physical ocean circulation processes

Corresponding author: Samuel C Mogen, samuel.mogen@colorado.edu

Abstract

The Blob was a marine heat wave in the Northeast Pacific from 2013 to 2016. While the upper ocean temperature in the Blob has been well described, the impacts on marine biogeochemistry have not been fully studied. Here, we characterize and develop understanding of Eastern North Pacific upper ocean biogeochemical properties during the Winter of 2013-14 using in situ observations, an observation-based product, and reconstructions from a collection of ocean models. We find that the Blob is associated with significant upper ocean biogeochemical anomalies: a 5% increase in aragonite saturation state (temporary reprieve of ocean acidification) and a 3% decrease in oxygen concentration (enhanced deoxygenation). Anomalous advection and mixing drives the aragonite saturation anomaly, while anomalous heating and air-sea gas exchange drive the oxygen anomaly. Marine heatwaves do not necessarily serve as an analog for future change as they may enhance or mitigate long-term trends.

Plain Language Summary

The global ocean is experiencing major changes due to human-made carbon emissions and climate change, leading to a warming ocean with increasing acidity and declining oxygen. On top of these long-term changes in the ocean are short-term extreme events, such as marine heatwaves. These extreme events quickly change the ocean state and can stress marine ecosystems in multiple ways. The North Pacific Blob (2013-2016) was one such marine heatwave. While the ocean temperature changes during the event are well understood, the effects on ocean biogeochemistry have not been fully examined. In this study, we use an earth system model that accurately simulates the Blob to examine short-term changes in oxygen and acidity. We find that the warming signal leads to a decline in the effects of ocean acidification, mainly due to changes in the movement of carbon, and lowers the amount of oxygen, due primarily to temperature-driven effects. These results suggest that some effects of climate change will be exacerbated (warming) or mitigated (ocean acidification) by marine heatwaves.

1 Introduction

Anthropogenic climate change is leading to simultaneous warming, deoxygenation, and acidification stress on marine ecosystems [*Doney et al.*, 2009; *Bopp et al.*, 2013; *Kwiatkowski et al.*, 2020]. The North Pacific Ocean is particularly vulnerable to the effects of ocean acidification and deoxygenation, owing to the naturally high concentrations of dissolved inorganic carbon (DIC) and naturally low oxygen concentrations that occur here [*Ono et al.*, 2019; *Keeling et al.*, 2010; *Levin*, 2018]. On top of these long-term changes in ocean state are short-term extreme events defined by rapid disruptions such as marine heatwaves, which also likely have biogeochemical signatures [*Bopp et al.*, 2013; *Frölicher and Laufkötter*, 2018]. The North Pacific is thus especially threatened by these ecosystem multi-stressor or compound extreme events.

A strong marine heatwave known as "the Blob" appeared in the open Gulf of Alaska (GOA) in the winter of 2013-2014, driven by an anomalous high pressure ridge [*Bond et al.*, 2015; *Di Lorenzo and Mantua*, 2016; *Bif et al.*, 2019]. The anomalous high pressure system was associated with a significant decline in local wind speed, decreasing the mixing of deep, cold waters to the surface and raising sea surface temperatures [*Bond et al.*, 2015; *Scannell et al.*, 2020]. *Di Lorenzo and Mantua* [2016] proposed that the initial manifestation of the Blob (winter 2014) mapped onto the pattern of the North Pacific Gyre Oscillation (NPGO) [NGPGO; *Di Lorenzo et al.*, 2008] in the open GOA and transitioned to a Pacifical Decadal Oscilliation (PDO)-like pattern in the winter of 2015 due to tropical and extra-tropical teleconnections related to El Niño-Southern Oscillation (ENSO) [PDO; *Mantua et al.*, 1997]. This climatic transition transformed the Blob from a circle-like manifestation in the open GOA to an arc-shaped pattern along the coast that intersected with the California Current System (CCS) [*Di Lorenzo and Mantua*, 2016].

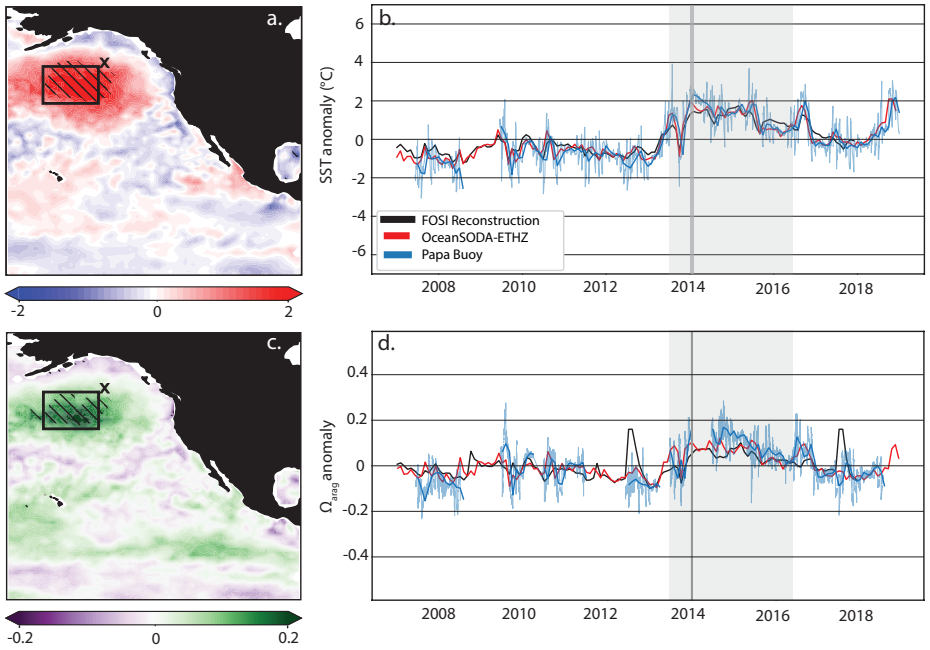

Figure 1. Physical and biogeochemical signatures of the Blob. Detrended anomalies in (a) sea surface temperature, and (c) Ω_{arag} in Jan-Feb 2014 relative to a base period Jan-Feb 1985-2010 from the OceanSODA-ETHZ observation-based product. Stippling indicates statistical significance at the 2σ level. Black box indicates the area defined by 40-50°N and 145-160°W. Temporal evolution of the monthly deseasoned and detrended anomalies in surface ocean (b) temperature, and (d) Ω_{arag} at the Papa Buoy (x in panels a and c) over 2007-2019 from the (black) CESM-FOSI reconstruction, (red) OceanSODA-ETHZ observation-based product, (blue) Papa buoy at monthly resolution, (light blue) Papa buoy at 3-hourly resolution (nearest grid cell in both gridded products). Gray shading indicates the 2013-2016 blob period, and gray vertical line indicates the peak blob intensity in the GOA region.

While the temperature features of the Blob have been well studied, only a few studies have discussed the ocean biogeochemical properties associated with the Blob. At the basin scale, the Blob has been connected to decreases in net community production [*Bif et al.*, 2019], increases in particulate organic carbon concentration and net primary productivity [*Yu et al.*, 2019; *Long et al.*, 2021], and changes to northeast Pacific fish stocks [*Cheung and Frölicher*, 2020]. Coastal biogeochemical impacts of the Blob include anomalously low chlorophyll concentrations off the coast of Southern California [*Kahru et al.*, 2018; *Jacox et al.*, 2016], anomalously high surface ocean partial pressure of CO_2 (pCO_2) off the coast of Washington state [*Siedlecki et al.*, 2016], and anomalously high aragonite saturation states (Ω_{arag}) off the coast of Alaska [*Siedlecki et al.*, 2016]. While these studies suggest basin-wide and/or coastal impacts of the Blob on individual ocean biogeochemical parameters, no study has comprehensively analyzed the impact of the Blob on multiple biogeochemical parameters in the open GOA, where the Blob exhibited its most intense temperature anomaly in the winter of 2013-14.

Here, we characterize the biogeochemistry of the North Pacific Blob in the open GOA during the winter of 2013-14, at the location and time of the most intense surface temperature anomaly. We use a collection of ocean observations and model output to quantify carbonate chemistry and oxygen anomalies in the surface ocean and attribute them to anomalous physical forcing of the coupled air-sea system. Our results demonstrate that this region's response to the Blob was characterized by a relief of ocean acidification (i.e., anomalously high aragonite saturation states), but an intensification of deoxygenation.

2 Methods

2.1 Ocean model reconstructions

Our primary numerical tool is a historical reconstruction of the ocean physical and biogeochemical state generated by a Forced Ocean-Sea Ice (FOSI) configuration of the Community Earth System Model (CESM). CESM FOSI consists of coupled ocean and sea ice components of CESM1.1 forced with historical (1948-2017) atmospheric state and flux fields from the Coordinated Ocean-Ice Reference Experiment (CORE) dataset. This configuration of CESM has been shown to reproduce key aspects of observed ocean variability [*Yeager et al.*, 2018]. CESM1.1 simulates the ocean at $1^\circ \times 1^\circ$ resolution with 60 vertical levels using version 2 of the Parallel Ocean Program (POP) with an explicit rendering of marine biogeochemistry from the Biogeochemistry Elemental Cycle (BEC) model [*Moore et al.*, 2001, 2004, 2013]. BEC includes three explicit phytoplankton functional groups (diatoms, diazotrophs, and picophytoplankton) and one implicit group (calcifiers) along with one group of zooplankton [*Moore et al.*, 2004]. BEC also includes multiple nutrient limitations (N, P, Si, Fe) and a fully realized marine carbonate system [*Moore et al.*, 2001, 2004, 2013]. CESM FOSI produces physical and biogeochemical output on monthly timescales.

The Ocean Model Intercomparison Project (OMIP) provides experimental protocols for coupled ocean and sea-ice models forced with strongly constrained air-sea momentum, heat, and freshwater fluxes derived from atmospheric reanalysis fields [*Griffies et al.*, 2016; *Orr et al.*, 2017; *Tsujino et al.*, 2020]. Since the simulations belonging to the first phase of the OMIP (OMIP-1) end in 2009, we use a subset of models based on phase 2 (OMIP-2) that include biogeochemical tracers and provide output to the CMIP6 archive at monthly resolution: NorESM and MRI. OMIP2 simulations capture the anomalous momentum, heat, and freshwater fluxes present during the Blob period (2013-2016) [*Griffies et al.*, 2016]. NorESM-LM is the second generation Earth System Model developed by the Norwegian Climate Center [*Seland et al.*, 2020]. We also analyzed OMIP2 output from the Meteorological Research Institute of Japan Earth System Model version 2.0 (MRI-ESM2.0) [*Yukimoto et al.*, 2019]. As MRI did not provide aragonite saturation state to the OMIP/CMIP6 archive, we calculated Ω_{arag} by assuming a surface ocean saturation value ($[CO_3^{2-}]_{sat,arag}$) of 65.0 μmol kg^{-1} everywhere [*Sarmiento and Gruber*, 2006] in equation 1:

$$\Omega_{aragonite} = \frac{[CO_3^{2-}]}{[CO_3^{2-}]_{sat,arag}} \quad (1)$$

2.2 Observations

We also examine the Blob via observations collected at Ocean Station Papa and a global observation-based product (OceanSODA ETHZ). Ocean Station Papa, one of over 50 moorings globally with Moored Autonomous pCO_2 (MAPCO2) systems, has collected physical, pCO_2, and oxygen data since 2007 [*Sutton et al.*, 2014, 2012; *Emerson et al.*, 2017]. The buoy is located in the open GOA at 50.1 ° N, 144.9 ° W (x in Figure 1a), immediately adjacent to the region with the most intense surface ocean heating in the winter of 2014. We estimated total alkalinity (Alk) at the Papa buoy using equation 2 from *Fassbender et al.* [2016],

$$\text{Alk} = 37 \cdot \text{S} + 988, \quad (2)$$

where salinity (S) is derived from in situ buoy measurements. Estimated alkalinity and in-situ buoy pCO_2 measurements were used to solve the full carbonate system in PYCO2sys, a python toolbox based on the CO2SYS program [*Humphreys et al.*, 2021a]. PYCO2sys has been validated and shown to produce results similar to other carbonate system solvers [*Humphreys et al.*, 2021b]. PYCO2SYS estimates equilibrium constants based on temperature, salinity, and pressure with program default versions of all constants based on *Sulpis et al.* [2020].

OceanSODA-ETHZ was developed by interpolating surface pCO_2 from the Surface Ocean CO_2 Atlas [SOCAT; *Bakker et al.*, 2016] and Alk from the Global Ocean Data Analysis Project [GLODAP2; *Olsen et al.*, 2019] observations with the Geospatial Random Cluster Ensemble Regression (GRaCER) method [*Gregor and Gruber*, 2021]. This product accurately reproduces the full ocean carbonate system [*Gregor and Gruber*, 2021].

2.3 Data Analysis

All model output was regridded to a regular $1° \times 1°$ grid using the Climate Data Operator (CDO) [*Schulzweida*, 2020]. The seasonal climatology was removed from all data and a second order polynomial fit was used to detrend the anomalies (as atmospheric CO_2 time series are approximated by a second order polynomial). The initial winter manifestation of the blob (January-February, 2014) was compared to a base period (January-February, 1985-2010) to determine the magnitude of the anomalies. Blob signals are deemed significantly different than the base period if they exceed 2-standard deviations (95% confidence interval for a normal distribution).

3 Results

The Blob period (2013-2016) is characterized by anomalously warm SSTs, anomalously high surface ocean Ω_{arag} and anomalously low surface oxygen concentrations in the Northeast Pacific Ocean (Figure 1, Supplemental Figure S1). In-situ observations from the Papa buoy show the development of the Blob SST signature near the beginning of 2014, with a rapid increase of ~2°C (Figure1b). The Papa buoy recorded a ~0.1 increase in Ω_{arag} and a ~4-5 mmol O_2 m^{-3} decrease in oxygen concentration in late 2013 (Figure 1d, Supplemental Figure S1). Unfortunately, a large gap in the buoy observational record precludes a quantification of the observed Ω_{arag} anomalies in the open GOA at the peak of the Blob in the winter of 2013-14 (Figure 1b,d).

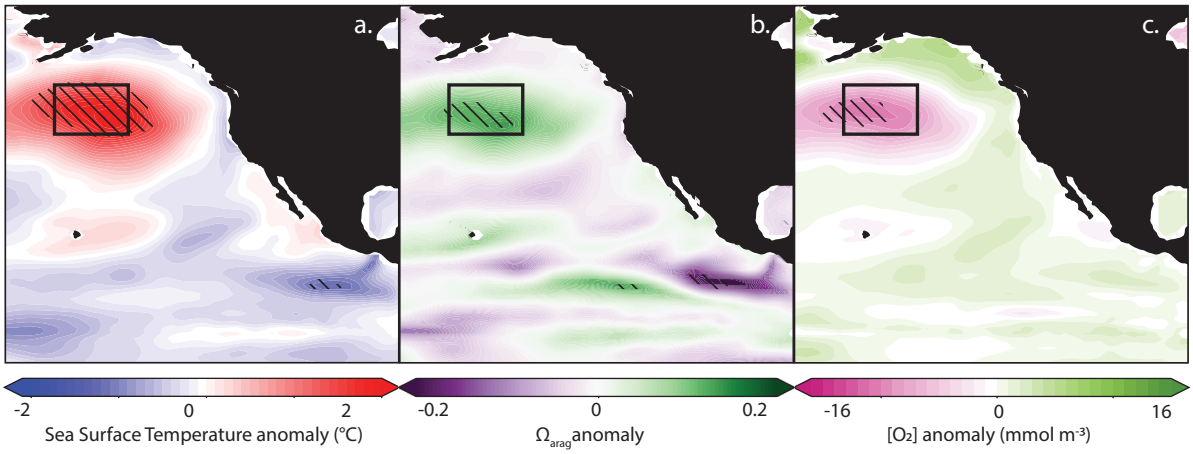

Figure 2. Physical and biogeochemical signatures of the Blob in the CESM Forced Ocean Sea Ice (FOSI) reconstruction. Detrended anomalies in (a) sea surface temperature, (b) surface Ω_{arag}, and (c) surface dissolved oxygen in Jan-Feb 2014 relative to a base period Jan-Feb 1985-2010. Stippling indicates statistical significance at the 2σ level. Black box indicates the region of study for the GOA manifestation of the Blob

The positive Blob anomaly in surface $\Omega_{aragonite}$ spans the full GOA during the winter of 2014, as illustrated by the interpolated OceanSODA ETHZ observation-based product (Figure 1c). The detrended Ω_{arag} anomalies in Jan-Feb 2014 map onto the SST anomalies during the same period (cf. Figures 1a and c), indicating an important role for physical processes in driving Blob biogeochemical anomalies in the open GOA region. The temporal evolution of the SST and Ω_{arag} anomalies from the OceanSODA ETHZ product display high correlations with Papa buoy data over 2007-2018 and suggest that the largest anomalies in SST and Ω_{arag} occurred in Jan-Feb 2014 (order 2°C and 0.1, respectively; Figure 1b,d).

CESM FOSI accurately recreates the physical and biogeochemical signatures of the Blob as estimated by in-situ and interpolated observations and other ocean physical-biogeochemical models. Figures 1b,d show that FOSI captures the same timeseries anomaly in both SST ($\sim$ 1°C) and Ω_{arag} ($\sim$ 0.05) during the Blob period, while Supplemental Figure S1 shows that the Blob-associated oxygen anomaly is well captured in comparison to in-situ observations (decline of $\sim$ 4-5 mmol O_2 m^{-3}). The average anomalies in surface temperature, Ω_{arag}, and oxygen over the full Blob period (7/2013 – 6/2016) at the location of the Papa buoy are of similar magnitude for FOSI, the interpolated reconstruction, and the buoy data (Table S1). In the open GOA region (black box in Figure 1) during the winter of 2013-14, the FOSI reconstruction again produces anomalies similar to those in the observation-based product (Table S2). The magnitude and spatial extent of the surface temperature and Ω_{arag} anomalies during the winter of 2014 are similar across the CESM FOSI, MRI OMIP2, and NorESM OMIP2 simulations (cf. Figure 2 and Figure S2), indicating that these signatures are relatively insensitive to model structure and forcing dataset. Oxygen anomaly magnitudes are similar in both observations and CESM FOSI but much smaller in MRI OMIP2 and NorESM OMIP2 simulations.

What caused the temporary reprieve of ocean acidification (anomalously high Ω_{arag}) during the winter of 2013-14 in the open GOA? We use output from CESM-FOSI to develop a mechanistic understanding of the positive anomaly in surface ocean Ω_{arag} in the GOA Blob region during Jan-Feb 2014. Ω_{arag} is equal to the carbonate ion concentration, $[CO_3^{2-}]$, divided by the carbonate ion concentration in saturation with mineral aragonite,

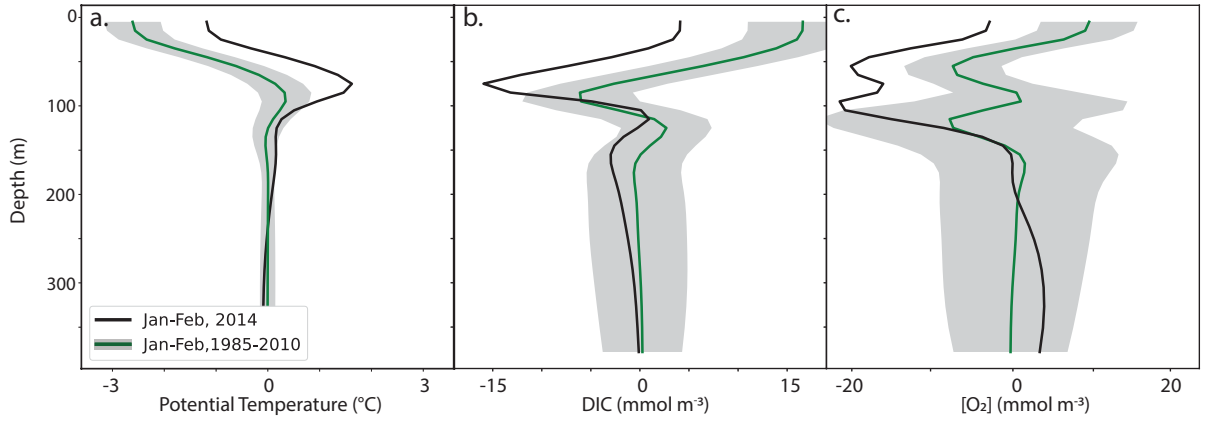

Figure 3. Vertical structure of the Blob from the CESM Forced Ocean Sea Ice (FOSI) Reconstruction. Detrended vertical profiles of (a) potential temperature, (b) DIC, and (c) oxygen concentration in the GOA box during (black) Jan-Feb 2014 and (green/gray) Jan-Feb 1985-2010 with one standard deviation.

$[CO_3^{2-}]_{sat,arag}$ (Equation 1), and determines the tendency for aragonite shells to precipitate ($\Omega_{arag} > 1$) or dissolve ($\Omega_{arag} < 1$). As $[CO_3^{2-}]_{sat,arag}$ is largely unmodified in the Blob (not shown), anomalies in Ω_{arag} derive from anomalies in $[CO_3^{2-}]$. We decompose the surface ocean $[CO_3^{2-}]$ Blob anomalies into contributions from anomalies in surface temperature (T), salinity (S), salinity-normalized DIC (sDIC), salinity-normalized alkalinity (sAlk), and freshwater dilution [*fw*; see Appendix A of *Lovenduski et al.*, 2015],

$$\Delta[CO_3^{2-}] = \frac{\partial[CO_3^{2-}]}{\partial T}\Delta T + \frac{\partial[CO_3^{2-}]}{\partial S}\Delta S + \frac{S}{35}\frac{\partial[CO_3^{2-}]}{\partial DIC}\Delta sDIC + \frac{S}{35}\frac{\partial[CO_3^{2-}]}{\partial Alk}\Delta sAlk + \frac{\partial[CO_3^{2-}]}{\partial fw}\Delta fw, \quad (3)$$

where the sensitivities are determined using a carbonate system solver and the Δ terms are the anomalies in the Blob. Results from this model decomposition demonstrate that a reduction in surface ocean DIC largely drives the temporary relief of ocean acidification in the open GOA during the winter of 2013-14 (Table 1). Other drivers, including alkalinity, SST, salinity, and freshwater dilution have smaller effects on the change in $[CO_3^{2-}]$ in the Blob region. The $[CO_3^{2-}]$ change estimated by the sum of the decomposed drivers successfully reproduces the modeled change in $[CO_3^{2-}]$ (Table 1).

The Blob-related DIC anomalies extend from the surface to a depth of 100 m in the open GOA during Jan-Feb 2014 in CESM FOSI (Figure 3b), mirroring anomalies in potential temperature (Figure 3a). The detrended mean anomaly profile of DIC exhibits a vertical gradient of ~15 mmol m^{-3} in the top 100 m, with a modest amount of interannual variation (Figure 3b). During the winter of 2014, DIC decreases significantly through the upper 100 m in the open GOA box, with nearly equal declines at every depth level. Thus, to develop a clear understanding of the Blob-induced changes in DIC, we need to consider the integrated DIC budget in the upper 100 m and the processes that affect DIC change here.

Blob anomalies in upper ocean DIC were examined as a function of the circulation, air-sea flux, and biological processes that affect the rate of change of DIC in our region of study (Figure 4a) using the following equation,

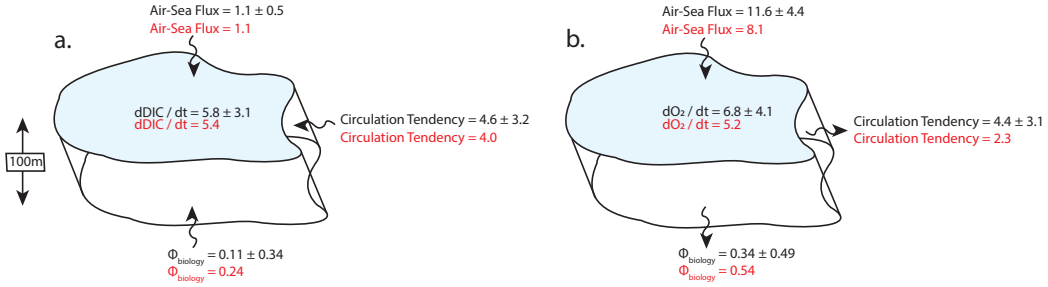

Figure 4. Drivers of changing biogeochemistry in the Blob. (a) Rate of change of salinity-normalized DIC in the upper 100 m of the Blob region during (black) the base period Jan-Feb 1985-2010 and (red) Jan-Feb 2014 (mol m^{-2} yr^{-1}). Fluxes of DIC driven by air-sea exchange, biological processes, and ocean circulation during the Blob and base period are indicated as arrows. Arrows into the box represent addition of carbon (positive) while arrows out of the box indicate loss of carbon (negative) (b) As in panel a, but for dissolved oxygen (mol m^{-2} yr^{-1}).

$$\frac{\partial DIC}{\partial t} = \Phi_{\text{biology}} + \text{Air Sea Flux} + \text{Circulation Tendency}, \tag{4}$$

where $\frac{\partial DIC}{\partial t}$ is saved at model run time, Φ_{biology} represents the flux of carbon into/out of the Blob box driven by organic matter production and remineralization, the air-sea flux captures changes in upper ocean DIC driven by gas exchange, and the circulation tendency representing advection and mixing is calculated as a residual.

Upper ocean Blob DIC anomalies are primarily driven by changes in circulation processes, with biological and air-sea fluxes playing less important roles (Figure 4a). The black text in Figure 4a indicates the rate of change of DIC, as well as the fluxes of DIC into/out of the Blob region driven by air-sea, circulation, and biological fluxes during a typical January-February period. DIC in the top 100 meters in the open GOA tends to increase in the winter months ($\frac{\partial DIC}{\partial t}$ = 5.8 ± 3.1 mol C m^{-2} yr^{-1}), driven almost entirely by the tendency of circulation to advect and mix DIC vertically and laterally into the region (4.6 ± 3.2 mol C m^{-2} yr^{-1}), with air-sea flux and biological remineralization adding slightly to this tendency (Figure 4a). During the winter of 2013-14, changes in the circulation tendency reduced the supply of DIC into the Blob region, which decreased the DIC concentration relative to its mean state (Figure 4a). This change in DIC circulation tendency is associated with an increase in density stratification in this region during the Blob (Supplemental Figure S4). The Blob also led to anomalies in biological carbon fluxes, but these were much smaller magnitude changes. These results are supportive of a stratification-driven decrease in DIC supply during the Blob in this region.

What processes are responsible for the decrease in the upper ocean oxygen concentration during the winter of 2013-14 in the open GOA in CESM FOSI (Figure 3c)? Detrended Blob anomalies in oxygen relative to the base period illustrate the vertical extent of oxygen anomalies during the Blob (Figure 3). While DIC is a conservative tracer and independent of temperature changes, oxygen is a dissolved gas whose concentration in seawater is highly sensitive to changes in temperature. To more closely examine the role of temperature in driving oxygen changes, we decompose the modeled Blob oxygen anomaly (ΔO_2) into temperature and non-temperature driven components,

$$\Delta O_2 = \frac{\partial O_2}{\partial T} \cdot \Delta T + \Delta O_{2,\text{non-T}}, \tag{5}$$

where the first term captures the temperature sensitivity component $\frac{\partial O_2}{\partial T}$ = -3.32 mmol O_2 $^\circ$ C $^{-1}$ and is determined via Equation 6 and Table 3.2.4 of *Sarmiento and Gruber* [2006], and the non-T term is the residual. This analysis reveals that the loss of oxygen in the open GOA during the winter of 2013-14 is primarily driven by temperature, with other processes playing only a small role (Figure S3). This finding is also reflected in the upper ocean oxygen budget for the Blob region (Figure 4b), where changes in air-sea oxygen flux due to solubility are largely responsible for the decreasing oxygen concentration, while changes in oxygen driven by circulation and biological processes play secondary roles. Thus, while ocean circulation changes and stratification (Sup. Fig. S4) brought on by anomalous upper ocean heating during the Blob reduced the DIC supply and temporarily relieved surface ocean acidification, this same upper ocean heating decreased the solubility of oxygen and led to temporary surface deoxygenation.

4 Conclusions and Discussion

Our research shows that the Northeast Pacific Blob was characterized by dramatic changes in regional marine biogeochemistry. In the open GOA during the winter of 2013-14 at peak Blob SST anomalies, we found significant increases in surface ocean Ω_{arag} and decreases in surface ocean oxygen concentrations. These biogeochemical anomalies extended to depths of 100 m and were ultimately driven by ocean stratification anomalies (in the case of Ω_{arag}) and temperature/solubility forcing (in the case of oxygen).

These results demonstrate that marine heat waves can have strong biogeochemical signals in the open ocean. In the case of the Blob, the heat wave was associated with a temporary mitigation of acidification but an exacerbation of deoxygenation in the open GOA, aligning with Blob-associated biogeochemical anomalies in coastal regions [e.g., *Siedlecki et al.*, 2016]. As an investigation of multiple ecosystem stressors or compound events, this study indicates that the Blob stressed the ecosystem with both high temperatures and reduced oxygen concentrations, but that organisms that perform calcification may have experienced some benefits from the event. As such, our work demonstrates that marine heatwaves do not necessarily lead to universally worse environmental conditions for sensitive marine ecosystems. They also do not necessarily serve as analogs for future climate change, as the temporary changes induced by marine heatwaves may enhance or mitigate long-term trends, depending on the variable of interest.

These results are a promising start to understanding the multiple stressors impacting the ocean during marine heat waves which have vast impacts on marine ecosystems. Future work should investigate other marine heatwaves from an observational and modeling perspective to better understand the risks to the marine ecosystem. Newly-developed seasonal-to-decadal predictive model simulations also offer the chance to identify and predict extremes in advance, which may allow for adaptive marine resource management in the future.

Open Research

The CESM simulation data analyzed in this paper are available from the project web page of the CESM Decadal Prediction Large Ensemble (http://www.cesm.ucar.edu/ projects/community-projects/DPLE/). OceanSODA-ETHZ can be found at https://doi.org/10.25921/m5wx-ja34. OMIP2 model data have been generated as part of the internationally-coordinated Coupled Model Intercomparison Project Phase 6 (CMIP6; see also GMD Special Issue: http://www.geosci-model-dev.net/special_issue590.html). The project includes simulations from about 120 global climate models and around 45 institutions and organizations worldwide. - Project

website: https://pcmdi.llnl.gov/CMIP6. Data from the Papa Buoy can found for oxygen (https://www.ncei.noaa.gov/data/oceans/ncei/ocads/metadata/0160486.html) and carbon (https://www.ncei.noaa.gov/data/oceans/ncei/ocads/data/0100074/).

Acknowledgments

This research was supported by the National Oceanic and Atmospheric Administration (NA20OAR4310405) and the National Science Foundation (OCE 1752724). Ocean Station Papa buoy observations are supported by the Office of Oceanic and Atmospheric Research of NOAA, US Department of Commerce, including resources from the Global Ocean Monitoring and Observing Program and the Ocean Acidification Program. We thank the World Climate Research Program for developing CMIP6 and making model output available in the CMIP6 Archive and ETH Zurich for developing OceanSODA-ETHZ (the latter was funded by the European Commission through the COMFORT project; grant no. 820989). This is PMEL contribution 5316.

References

Bakker, D. C. E., B. Pfeil, C. S. Landa, N. Metzl, K. M. O'Brien, A. Olsen, K. Smith, C. Cosca, S. Harasawa, S. D. Jones, S.-i. Nakaoka, Y. Nojiri, U. Schuster, T. Steinhoff, C. Sweeney, T. Takahashi, B. Tilbrook, C. Wada, R. Wanninkhof, S. R. Alin, C. F. Balestrini, L. Barbero, N. R. Bates, A. A. Bianchi, F. Bonou, J. Boutin, Y. Bozec, E. F. Burger, W.-J. Cai, R. D. Castle, L. Chen, M. Chierici, K. Currie, W. Evans, C. Featherstone, R. A. Feely, A. Fransson, C. Goyet, N. Greenwood, L. Gregor, S. Hankin, N. J. Hardman-Mountford, J. Harlay, J. Hauck, M. Hoppema, M. P. Humphreys, C. W. Hunt, B. Huss, J. S. P. Ibánhez, T. Johannessen, R. Keeling, V. Kitidis, A. Körtzinger, A. Kozyr, E. Krasakopoulou, A. Kuwata, P. Landschützer, S. K. Lauvset, N. Lefèvre, C. Lo Monaco, A. Manke, J. T. Mathis, L. Merlivat, F. J. Millero, P. M. S. Monteiro, D. R. Munro, A. Murata, T. Newberger, A. M. Omar, T. Ono, K. Paterson, D. Pearce, D. Pierrot, L. L. Robbins, S. Saito, J. Salisbury, R. Schlitzer, B. Schneider, R. Schweitzer, R. Sieger, I. Skjelvan, K. F. Sullivan, S. C. Sutherland, A. J. Sutton, K. Tadokoro, M. Telszewski, M. Tuma, S. M. A. C. van Heuven, D. Vandemark, B. Ward, A. J. Watson, and S. Xu (2016), A multi-decade record of high-quality pCO2 data in version 3 of the Surface Ocean CO2; Atlas (SOCAT), *Earth System Science Data*, *8*(2), 383–413, doi:10.5194/essd-8-383-2016.

Bif, M. B., L. Siqueira, and D. A. Hansell (2019), Warm Events Induce Loss of Resilience in Organic Carbon Production in the Northeast Pacific Ocean, *Global Biogeochemical Cycles*, *33*(9), 1174–1186, doi:10.1029/2019GB006327.

Bond, N. A., M. F. Cronin, H. Freeland, and N. Mantua (2015), Causes and impacts of the 2014 warm anomaly in the NE Pacific: 2014 WARM ANOMALY IN THE NE PACIFIC, *Geophysical Research Letters*, *42*(9), 3414–3420, doi:10.1002/2015GL063306.

Bopp, L., L. Resplandy, J. C. Orr, S. C. Doney, J. P. Dunne, M. Gehlen, P. Halloran, C. Heinze, T. Ilyina, R. Séférian, J. Tjiputra, and M. Vichi (2013), Multiple stressors of ocean ecosystems in the 21st century: projections with CMIP5 models, *Biogeosciences*, *10*(10), 6225–6245, doi:10.5194/bg-10-6225-2013.

Cheung, W. W. L., and T. L. Frölicher (2020), Marine heatwaves exacerbate climate change impacts for fisheries in the northeast Pacific, *Scientific Reports*, *10*(1), 6678, doi:10.1038/s41598-020-63650-z.

Di Lorenzo, E., and N. Mantua (2016), Multi-year persistence of the 2014/15 North Pacific marine heatwave, *Nature Climate Change*, *6*(11), 1042–1047, doi:10.1038/nclimate3082.

Di Lorenzo, E., N. Schneider, K. M. Cobb, P. J. S. Franks, K. Chhak, A. J. Miller, J. C. McWilliams, S. J. Bograd, H. Arango, E. Curchitser, T. M. Powell, and P. Rivière (2008), North Pacific Gyre Oscillation links ocean climate and ecosystem change, *Geophysical Research Letters*, *35*(8), L08,607, doi:10.1029/2007GL032838.

Doney, S. C., V. J. Fabry, R. A. Feely, and J. A. Kleypas (2009), Ocean Acidification: The Other CO $_2$ Problem, *Annual Review of Marine Science*, *1*(1), 169–192, doi:

10.1146/annurev.marine.010908.163834.

Emerson, S., M. R. T. White, C. L. Stump, and S. M. Bushinsky (2017), Salinity and other variables collected from time series observations using Bubble type equilibrator for autonomous carbon dioxide (CO2) measurement, Carbon dioxide (CO2) gas analyzer and other instruments from MOORINGS_papa_145w_50n in the North Pacific Ocean from 2007-06-08 to 2014-11-06 (NCEI Accession 0160486), doi: 10.3334/CDIAC/OTG.TSM_PAPA_145W_50N_O2_N2, type: dataset.

Fassbender, A. J., C. L. Sabine, and M. F. Cronin (2016), Net community production and calcification from 7 years of NOAA Station Papa Mooring measurements, *Global Biogeochemical Cycles*, *30*(2), 250–267, doi:10.1002/2015GB005205.

Frölicher, T. L., and C. Laufkötter (2018), Emerging risks from marine heat waves, *Nature Communications*, *9*(1), 650, doi:10.1038/s41467-018-03163-6.

Gregor, L., and N. Gruber (2021), OceanSODA-ETHZ: a global gridded data set of the surface ocean carbonate system for seasonal to decadal studies of ocean acidification, *Earth System Science Data*, *13*(2), 777–808, doi:10.5194/essd-13-777-2021.

Griffies, S. M., G. Danabasoglu, P. J. Durack, A. J. Adcroft, V. Balaji, C. W. Böning, E. P. Chassignet, E. Curchitser, J. Deshayes, H. Drange, B. Fox-Kemper, P. J. Gleckler, J. M. Gregory, H. Haak, R. W. Hallberg, P. Heimbach, H. T. Hewitt, D. M. Holland, T. Ilyina, J. H. Jungclaus, Y. Komuro, J. P. Krasting, W. G. Large, S. J. Marsland, S. Masina, T. J. McDougall, A. J. G. Nurser, J. C. Orr, A. Pirani, F. Qiao, R. J. Stouffer, K. E. Taylor, A. M. Treguier, H. Tsujino, P. Uotila, M. Valdivieso, Q. Wang, M. Winton, and S. G. Yeager (2016), OMIP contribution to CMIP6: experimental and diagnosticprotocol for the physical component of the Ocean Model Intercomparison Project, *Geoscientific Model Development*, *9*(9), 3231–3296, doi:10.5194/gmd-9-3231-2016.

Humphreys, M. P., E. R. Lewis, J. D. Sharp, and D. Pierrot (2021a), PyCO2SYS v1.7: marine carbonate system calculations in Python, *preprint*, Oceanography, doi:10.5194/gmd-2021-159.

Humphreys, M. P., A. J. Schiller, D. Sandborn, L. Gregor, D. Pierrot, S. M. A. C. van Heuven, E. R. Lewis, and D. W. R. Wallace (2021b), PyCO2SYS: marine carbonate system calculations in Python, doi:10.5281/zenodo.5176106.

Jacox, M. G., E. L. Hazen, K. D. Zaba, D. L. Rudnick, C. A. Edwards, A. M. Moore, and S. J. Bograd (2016), Impacts of the 2015–2016 El Niño on the California Current System: Early assessment and comparison to past events, *Geophysical Research Letters*, *43*(13), 7072–7080, doi:10.1002/2016GL069716.

Kahru, M., M. G. Jacox, and M. D. Ohman (2018), CCE1: Decrease in the frequency of oceanic fronts and surface chlorophyll concentration in the California Current System during the 2014–2016 northeast Pacific warm anomalies, *Deep Sea Research Part I: Oceanographic Research Papers*, *140*, 4–13, doi:10.1016/j.dsr.2018.04.007.

Keeling, R. F., A. Körtzinger, and N. Gruber (2010), Ocean Deoxygenation in a Warming World, *Annual Review of Marine Science*, *2*(1), 199–229, doi: 10.1146/annurev.marine.010908.163855.

Kwiatkowski, L., O. Torres, L. Bopp, O. Aumont, M. Chamberlain, J. R. Christian, J. P. Dunne, M. Gehlen, T. Ilyina, J. G. John, A. Lenton, H. Li, N. S. Lovenduski, J. C. Orr, J. Palmieri, Y. Santana-Falcón, J. Schwinger, R. Séférian, C. A. Stock, A. Tagliabue, Y. Takano, J. Tjiputra, K. Toyama, H. Tsujino, M. Watanabe, A. Yamamoto, A. Yool, and T. Ziehn (2020), Twenty-first century ocean warming, acidification, deoxygenation, and upper-ocean nutrient and primary production decline from CMIP6 model projections, *Biogeosciences*, *17*(13), 3439–3470, doi:10.5194/bg-17-3439-2020.

Levin, L. A. (2018), Manifestation, Drivers, and Emergence of Open Ocean Deoxygenation, *Annual Review of Marine Science*, *10*(1), 229–260, doi:10.1146/annurev-marine-121916-063359.

Long, J. S., A. J. Fassbender, and M. L. Estapa (2021), Depth-Resolved Net Primary Production in the Northeast Pacific Ocean: A Comparison of Satellite and Profiling Float Estimates in the Context of Two Marine Heatwaves, *Geophysical Research Letters*, *48*(19),

doi:10.1029/2021GL093462.

Lovenduski, N. S., M. C. Long, and K. Lindsay (2015), Natural variability in the surface ocean carbonate ion concentration, *Biogeosciences*, *12*(21), 6321–6335, doi:10.5194/bg-12-6321-2015.

Mantua, N. J., S. R. Hare, Y. Zhang, J. M. Wallace, and R. C. Francis (1997), A Pacific Interdecadal Climate Oscillation with Impacts on Salmon Production, *Bulletin of the American Meteorological Society*, *78*(6), 1069–1079, doi:10.1175/1520-0477(1997)078<1069:APICOW>2.0.CO;2.

Moore, J., S. C. Doney, J. A. Kleypas, D. M. Glover, and I. Y. Fung (2001), An intermediate complexity marine ecosystem model for the global domain, *Deep Sea Research Part II: Topical Studies in Oceanography*, *49*(1-3), 403–462, doi:10.1016/S0967-0645(01)00108-4.

Moore, J. K., S. C. Doney, and K. Lindsay (2004), Upper ocean ecosystem dynamics and iron cycling in a global three-dimensional model: GLOBAL ECOSYSTEM-BIOGEOCHEMICAL MODEL, *Global Biogeochemical Cycles*, *18*(4), n/a–n/a, doi:10.1029/2004GB002220.

Moore, J. K., K. Lindsay, S. C. Doney, M. C. Long, and K. Misumi (2013), Marine Ecosystem Dynamics and Biogeochemical Cycling in the Community Earth System Model [CESM1(BGC)]: Comparison of the 1990s with the 2090s under the RCP4.5 and RCP8.5 Scenarios, *Journal of Climate*, *26*(23), 9291–9312, doi:10.1175/JCLI-D-12-00566.1.

Olsen, A., N. Lange, R. M. Key, T. Tanhua, M. Álvarez, S. Becker, H. C. Bittig, B. R. Carter, L. Cotrim da Cunha, R. A. Feely, S. van Heuven, M. Hoppema, M. Ishii, E. Jeansson, S. D. Jones, S. Jutterström, M. K. Karlsen, A. Kozyr, S. K. Lauvset, C. Lo Monaco, A. Murata, F. F. Pérez, B. Pfeil, C. Schirnick, R. Steinfeldt, T. Suzuki, M. Telszewski, B. Tilbrook, A. Velo, and R. Wanninkhof (2019), GLODAPv2.2019 – an update of GLODAPv2, *Earth System Science Data*, *11*(3), 1437–1461, doi:10.5194/essd-11-1437-2019.

Ono, H., N. Kosugi, K. Toyama, H. Tsujino, A. Kojima, K. Enyo, Y. Iida, T. Nakano, and M. Ishii (2019), Acceleration of Ocean Acidification in the Western North Pacific, *Geophysical Research Letters*, *46*(22), 13,161–13,169, doi:10.1029/2019GL085121.

Orr, J. C., R. G. Najjar, O. Aumont, L. Bopp, J. L. Bullister, G. Danabasoglu, S. C. Doney, J. P. Dunne, J.-C. Dutay, H. Graven, S. M. Griffies, J. G. John, F. Joos, I. Levin, K. Lindsay, R. J. Matear, G. A. McKinley, A. Mouchet, A. Oschlies, A. Romanou, R. Schlitzer, A. Tagliabue, T. Tanhua, and A. Yool (2017), Biogeochemical protocols and diagnostics for the CMIP6 Ocean Model Intercomparison Project (OMIP), *Geoscientific Model Development*, *10*(6), 2169–2199, doi:10.5194/gmd-10-2169-2017.

Sarmiento, J. L., and N. Gruber (2006), *Ocean biogeochemical dynamics*, Princeton University Press, Princeton, oCLC: ocm60651167.

Scannell, H. A., G. C. Johnson, L. Thompson, J. M. Lyman, and S. C. Riser (2020), Subsurface Evolution and Persistence of Marine Heatwaves in the Northeast Pacific, *Geophysical Research Letters*, *47*(23), doi:10.1029/2020GL090548.

Schulzweida, U. (2020), CDO User Guide, doi:10.5281/ZENODO.4246983, publisher: Zenodo Version Number: 1.9.9.

Seland, O., M. Bentsen, D. Olivié, T. Toniazzo, A. Gjermundsen, L. S. Graff, J. B. Debernard, A. K. Gupta, Y.-C. He, A. Kirkevåg, J. Schwinger, J. Tjiputra, K. S. Aas, I. Bethke, Y. Fan, J. Griesfeller, A. Grini, C. Guo, M. Ilicak, I. H. H. Karset, O. Landgren, J. Liakka, K. O. Moseid, A. Nummelin, C. Spensberger, H. Tang, Z. Zhang, C. Heinze, T. Iversen, and M. Schulz (2020), Overview of the Norwegian Earth System Model (NorESM2) and key climate response of CMIP6 DECK, historical, and scenario simulations, *Geoscientific Model Development*, *13*(12), 6165–6200, doi:10.5194/gmd-13-6165-2020.

Siedlecki, S., E. Bjorkstedt, R. Feely, A. Sutton, J. Cross, and J. Newton (2016), Impact of the Blob on the Northeast Pacific Ocean, *US CLIVAR*, *14*(2), 6.

Sulpis, O., S. K. Lauvset, and M. Hagens (2020), Current estimates of K* and K* appear inconsistent with measured CO2 system parameters in cold oceanic regions, *Ocean Science*,

16(4), 847–862, doi:10.5194/os-16-847-2020.

Sutton, A. J., C. L. Sabine, C. Dietrich, S. Maenner Jones, S. Musielewicz, R. Bott, and J. Osborne (2012), High-resolution ocean and atmosphere pCO2 time-series measurements from mooring Papa_145w_50n in the North Pacific Ocean (NCEI Accession 0100074), doi:10.3334/CDIAC/OTG.TSM_PAPA_145W_50N, type: dataset.

Sutton, A. J., C. L. Sabine, S. Maenner-Jones, N. Lawrence-Slavas, C. Meinig, R. A. Feely, J. T. Mathis, S. Musielewicz, R. Bott, P. D. McLain, H. J. Fought, and A. Kozyr (2014), A high-frequency atmospheric and seawater pCO2 data set from 14 open-ocean sites using a moored autonomous system, *Earth System Science Data*, p. 14.

Tsujino, H., L. S. Urakawa, S. M. Griffies, G. Danabasoglu, A. J. Adcroft, A. E. Amaral, T. Arsouze, M. Bentsen, R. Bernardello, C. W. Böning, A. Bozec, E. P. Chassignet, S. Danilov, R. Dussin, E. Exarchou, P. G. Fogli, B. Fox-Kemper, C. Guo, M. Ilicak, D. Iovino, W. M. Kim, N. Koldunov, V. Lapin, Y. Li, P. Lin, K. Lindsay, H. Liu, M. C. Long, Y. Komuro, S. J. Marsland, S. Masina, A. Nummelin, J. K. Rieck, Y. Ruprich-Robert, M. Scheinert, V. Sicardi, D. Sidorenko, T. Suzuki, H. Tatebe, Q. Wang, S. G. Yeager, and Z. Yu (2020), Evaluation of global ocean–sea-ice model simulations based on the experimental protocols of the Ocean Model Intercomparison Project phase 2 (OMIP-2), *Geoscientific Model Development*, *13*(8), 3643–3708, doi:10.5194/gmd-13-3643-2020.

Yeager, S. G., G. Danabasoglu, N. A. Rosenbloom, W. Strand, S. C. Bates, G. A. Meehl, A. R. Karspeck, K. Lindsay, M. C. Long, H. Teng, and N. S. Lovenduski (2018), Predicting Near-Term Changes in the Earth System: A Large Ensemble of Initialized Decadal Prediction Simulations Using the Community Earth System Model, *Bulletin of the American Meteorological Society*, *99*(9), 1867–1886, doi:10.1175/BAMS-D-17-0098.1.

Yu, J., X. Wang, H. Fan, and R.-H. Zhang (2019), Impacts of Physical and Biological Processes on Spatial and Temporal Variability of Particulate Organic Carbon in the North Pacific Ocean during 2003–2017, *Scientific Reports*, *9*(1), 16,493, doi:10.1038/s41598-019-53025-4.

Yukimoto, S., H. Kawai, T. Koshiro, N. Oshima, K. Yoshida, S. Urakawa, H. Tsujino, M. Deushi, T. Tanaka, M. Hosaka, S. Yabu, H. Yoshimura, E. Shindo, R. Mizuta, A. Obata, Y. Adachi, and M. Ishii (2019), The Meteorological Research Institute Earth System Model Version 2.0, MRI-ESM2.0: Description and Basic Evaluation of the Physical Component, *Journal of the Meteorological Society of Japan. Ser. II*, *97*(5), 931–965, doi:10.2151/jmsj.2019-051.

Variable	Blob - Base
$\frac{\partial[CO_3^{2-}]}{\partial SST}\Delta SST$	0.64
$\frac{\partial[CO_3^{2-}]}{\partial S}\Delta S$	0.03
$\frac{S}{35}\frac{\partial[CO_3^{2-}]}{\partial DIC}\Delta sDIC$	7.36
$\frac{S}{35}\frac{\partial[CO_3^{2-}]}{\partial Alk}\Delta sAlk$	-1.81
$\frac{\partial[CO_3^{2-}]}{\partial fw}\Delta fw$	0.002
$^a\ \Delta\ [CO_3^{2-}]_{calculated}$	5.26
$^b\ \Delta[CO_3^{2-}]_{modeled}$	6.22

Table 1. Contributions to the anomaly in surface $[CO_3]$ in the open GOA (box in Figure 1) during Jan-Feb, 2014 relative to the base period (Jan-Feb, 1985-2010) from SST, surface salinity (S), salinity normalized DIC ($sDIC$), salinity normalized Alk ($sAlk$), and freshwater dilution (fw). Units are mmol m^{-3}. ^{a}The linear sum of the contributions. ^{b}The modeled anomaly in $[CO_3^{2-}]$.

Variable	Papa Buoy	OceanSODA-ETHZ	CESM FOSI
Δ SST	1.04	1.10	1.04
$\Delta\ \Omega_{arag}$	0.07	0.06	0.04
Δ [O_2]	-4.9	No data	-4.4

Table S1. Anomalies at the Papa Buoy Blob anomalies of Jan-Feb 2014 relative to a base period Jan-Feb 1985-2010 for SST, Ω_{arag}, and dissolved oxygen at the Papa Buoy during the full Blob period

Variable	OceanSODA-ETHZ	CESM FOSI	MRI	NorESM
Δ SST (°C)	1.93	1.41	1.91	1.8
$\Delta\ \Omega_{arag}$	0.16	0.10	0.09	0.10
Δ sDIC (mmol m^{-3})	-17.9	-12.6	No Data	No Data
Δ [O_2] (mmol m^{-3})	No data	-9.3	-0.01	-0.01

Table S2. Anomalies in SST, surface Ω_{arag}, and surface dissolved oxygen in the open GOA (box in Figure 1) during Jan-Feb, 2014.

Variable	Jan-Feb 1985-2010	Jan-Feb 2014
SST (^{o}C)	5.9	7.4
sDIC (mmol C m^{-3})	2177	2165
sAlk (mmol C m^{-3})	2355	2352
O_2 (mmol m^{-3})	295	286
$O_2{}^{T-residual}$ (mmol m^{-3})	289	285

Table S3. CESM-FOSI average surface values in the open GOA (black box in Figure 1) during Jan-Feb 1985-2010 and Jan-Feb 2014.

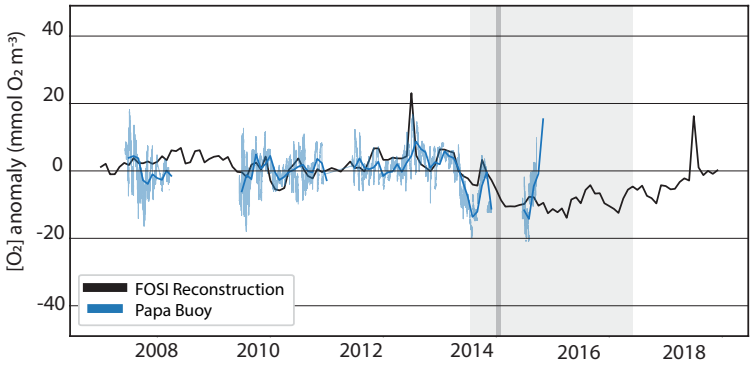

514 **Figure S1.** Temporal evolution of the deseasoned and detrended anomalies in surface ocean dissolved
515 oxygen at the location of the Papa Buoy over 2007-2019 from the (black) CESM-FOSI reconstruction, and
516 (blue) Papa buoy at monthly resolution, (light blue) Papa buoy at 3-hourly resolution (nearest grid cell in both
517 gridded products). Gray shading indicates the 2013-2016 blob period, and gray vertical line indicates the peak
518 blob intensity in the GOA region.

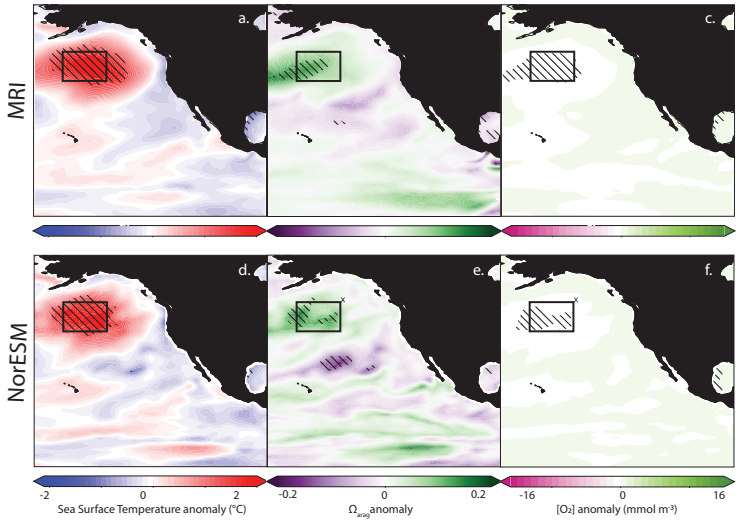

519 **Figure S2.** Detrended anomalies in (first column) sea surface temperature, (second column) surface Ω_{arag},
520 and (third column) surface dissolved oxygen in Jan-Feb 2014 relative to a base period Jan-Feb 1985-2010 for
521 (first row) MRI and (second row) NorESM. Stippling indicates statistical significance at the 2σ level.

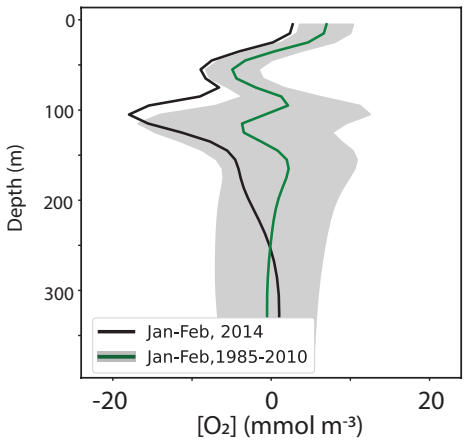

Figure S3. As in Figure 3c, but with temperature-driven oxygen signal removed.

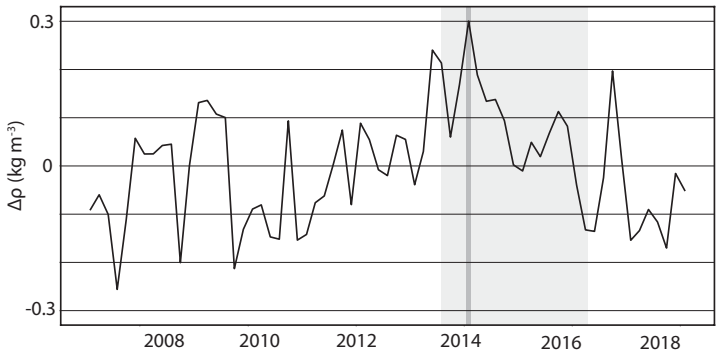

Figure S4. Density stratification in the blob Evolution of $\Delta\,\rho$ ($\rho_{210meters} - \rho_{5meters}$) in the initial blob box. Larger values indicate increase in regional stratification and a greater difference in vertical density levels.